

University of Nebraska - Lincoln

DigitalCommons@University of Nebraska - Lincoln

M. Eugene Rudd Publications

Research Papers in Physics and Astronomy

1-1996

Energy and Angular Distributions of Electrons from Ion Impact on Atomic and Molecular Hydrogen. III. 28–114-keV He⁺ + H₂

Y.-Y. Hsu

University of Nebraska - Lincoln

M. W. Gealy

University of Nebraska - Lincoln

G. W. Kerby III

University of Nebraska - Lincoln

M. Eugene Rudd

University of Nebraska - Lincoln, erudd@unl.edu

Follow this and additional works at: <https://digitalcommons.unl.edu/physicsrudd>

 Part of the [Physics Commons](#)

Hsu, Y.-Y.; Gealy, M. W.; Kerby III, G. W.; and Rudd, M. Eugene, "Energy and Angular Distributions of Electrons from Ion Impact on Atomic and Molecular Hydrogen. III. 28–114-keV He⁺ + H₂" (1996). *M. Eugene Rudd Publications*. 29.

<https://digitalcommons.unl.edu/physicsrudd/29>

This Article is brought to you for free and open access by the Research Papers in Physics and Astronomy at DigitalCommons@University of Nebraska - Lincoln. It has been accepted for inclusion in M. Eugene Rudd Publications by an authorized administrator of DigitalCommons@University of Nebraska - Lincoln.

Energy and angular distributions of electrons from ion impact on atomic and molecular hydrogen. III. 28–114-keV $\text{He}^+ + \text{H}_2$

Y.-Y. Hsu, M. W. Gealy,* G. W. Kerby III, and M. E. Rudd

Department of Physics and Astronomy, University of Nebraska, Lincoln, Nebraska 68588-0111

(Received 26 June 1995)

Absolute cross sections, differential in energy and angle of ejection of the secondary electrons, were determined for electron emission from $\text{He}^+ + \text{H}_2$ collisions at 28–114 keV by measuring electron energy spectra from 1.5 to 300 eV at several angles from 15° to 160° . A rotatable electrostatic analyzer was used with an energy resolution of 5% and an angular acceptance of 4.6° full width at half maximum. The double-differential cross sections were integrated over angle, energy, or both to obtain single-differential and total ionization cross sections. The latter are in excellent agreement with previous experimental results. Agreement of the experimental double-differential cross sections with plane-wave Born approximation calculations is generally poor. The cross section for ejection of high-energy electrons by He^+ is considerably larger than that for H^+ at the same velocity. This is attributed mostly to electron emission from the projectile. The presence of prominent Doppler-shifted helium autoionization peaks in the spectra indicates an appreciable probability for electron capture by the helium ions with simultaneous double excitation.

PACS number(s): 34.50.Fa

I. INTRODUCTION

Collisional ionization involving incident particles carrying orbital electrons has been studied experimentally and theoretically by several authors [1–5]. However, a detailed theoretical treatment of ionization by such projectiles at low energies is complicated by effects such as autoionization, electron loss from the projectile, electron capture to ground states, excited states, and continuum states, and by projectile-electron–target-electron interactions. Measurements of total ionization cross sections (TICS's) of H_2 for He^+ impact have been reported (e.g., Refs. [6–10]), but very little information about the angular and energy distribution of the ejected electrons is available. Electron energy spectra from $\text{He}^+ + \text{H}_2$ collisions were given by Oda and Nishimura [11] at 2 MeV and by Kövér *et al.* [12] at 3.2 MeV but both reported observations of electrons only at a single angle. The importance of detailed information such as that embodied in the double-differential cross sections (DDCS's) in understanding ionization processes was stressed in paper I [13]. Also explained there was the necessity of having data on H_2 targets in order to obtain the DDCS's for atomic hydrogen from experiments on mixed H and H_2 targets. The data for atomic hydrogen targets are presented in paper IV [14]. Since no DDCS data for $\text{He}^+ + \text{H}_2$ in this energy range had been previously reported, they had to be measured for this project and are presented here.

When the DDCS's are integrated over all directions of emission, the single-differential cross section (SDCS) $d\sigma/dW$ [also designated $\sigma(W)$] is obtained, where W is the ejected electron energy. If instead the DDCS is integrated over W , the SDCS $d\sigma/d\Omega$ [also designated $\sigma(\theta)$] results. Integrating over both angle and ejected electron energy, the TICS σ is obtained.

The contribution of projectile electrons to the observed spectrum was first studied by Wilson and Toburen [1], Burch, Wieman, and Ingalls [2], and Stolterfoht *et al.* [15]. Manson and Toburen [16] described electron emission from 2-MeV $\text{He}^+ + \text{He}$ collisions by including contributions from both the target and the projectile with and without simultaneous excitation of the other collision partner. All four of these combinations contributed appreciably to the cross sections for the 218-eV electrons studied.

II. EXPERIMENTAL METHOD

DDCS's were measured at eight angles from 15° to 160° for projectile energies from 28 to 114 keV. At each combination of incident energy and angle an energy spectrum was measured using a hemispherical electrostatic analyzer with an energy resolution of 5%. The full width at half maximum of the angular acceptance was 4.6° . Backgrounds were subtracted and the relative cross sections taken with a directed beam of H_2 were put on an absolute basis by measurements at each combination of primary-beam energy and electron ejection angle using a static gas target. The apparatus and experimental method were described in detail in paper I [13] so only the features and modifications relevant to this measurement will be described further here.

In the static gas measurements, corrections for electron absorption and beam neutralization were made as described earlier [13]. Cross sections used to make the neutralization correction were obtained from the compilation by McDaniel *et al.* [17]. Tests showed that the measured cross sections, corrected for these two effects, were insensitive to moderate changes in the target pressure and beam current. Typical uncertainties in the final DDCS's are 8% in the relative values and 18% in the absolute values. See paper I [13] for a more detailed discussion of reliability.

We examined the question of whether beam particles in excited states could have an effect on the measurement of ionization cross sections. States with $n < 9$ have lifetimes of

*Present address: Concordia College, Moorhead, MN 56562.

TABLE I. Measured values of $\sigma(W, \theta)$ in units of 10^{-20} cm²/eV sr, $\sigma(W)$ in units of 10^{-20} cm²/eV, $\sigma(\theta)$ in units of 10^{-20} cm²/sr, and σ_i (lower right-hand corner) in units of 10^{-20} cm² for secondary-electron production in 28-keV He⁺+H₂ collisions. Numbers in brackets are powers of 10 by which quantities are to be multiplied.

| W (eV) | 15° | 30° | 50° | 70° | 90° | 110° | 130° | 160° | $\sigma(W)$ |
|------------------|----------|----------|----------|----------|----------|----------|----------|----------|-------------|
| 1.5 | 727 | 152 | 110 | 72.1 | 58.0 | 52.1 | 51.4 | 51.9 | 1240 |
| 2 | 447 | 129 | 93.1 | 58.8 | 46.0 | 42.7 | 43.3 | 43.5 | 955 |
| 3 | 183 | 105 | 71.5 | 44.6 | 34.9 | 29.0 | 30.7 | 33.6 | 646 |
| 5 | 141 | 79.6 | 50 | 29.7 | 24.0 | 20.5 | 19.5 | 21.2 | 453 |
| 7.5 | 108 | 62.3 | 34.9 | 20.5 | 15.4 | 14.2 | 14.1 | 14.2 | 324 |
| 10 | 76.9 | 44.5 | 24.2 | 13.0 | 10.5 | 9.81 | 8.95 | 8.61 | 220 |
| 15 | 42.6 | 24 | 12.0 | 5.63 | 4.27 | 3.19 | 2.57 | 4.21 | 102 |
| 20 | 25 | 14.6 | 6.65 | 3.11 | 2.05 | 1.53 | 1.84 | 0.922 | 56.8 |
| 30 | 11.4 | 6.48 | 2.59 | 1.16 | 2.89 | 0.372 | 0.238 | 0.222 | 26.8 |
| 50 | 1.88 | 1.03 | 1.50 | 0.150 | 0.0719 | 0.0331 | 0.0259 | 0.0206 | 5.18 |
| 75 | 0.185 | 0.0832 | 0.0256 | 7.17[-3] | 5.12[-3] | 2.73[-3] | 4.31[-3] | 5.7[-3] | 0.262 |
| 100 | 0.0153 | 6.65[-3] | 2.34[-3] | 1.08[-3] | 5.18[-4] | 3.59[-4] | 2.70[-4] | 7.43[-4] | 0.0234 |
| 130 | 1.40[-3] | 6.28[-4] | 2.04[-4] | 8.78[-5] | 1.60[-4] | 1.35[-4] | 2.28[-4] | 3.17[-4] | 3.33[-3] |
| 160 | 9.74[-5] | 1.16[-4] | 1.4[-4] | | | | | 1.99[-4] | 6.49[-4] |
| 200 | 5.39[-5] | 1.65[-5] | | | | | | | 4.20[-5] |
| $\sigma(\theta)$ | 3780 | 1340 | 836 | 478 | 413 | 322 | 309 | 324 | 8170 |

the order of 10^{-8} s and, since the transit time was 1.6×10^{-6} s for even the highest-energy ions used, the fraction of such excited He⁺ ions reaching the collision center is less than 0.01%. An exception to this is the $2s$ metastable state which has a much longer lifetime in a field-free region. However, the electric field (which ranged from 600 to 2400 V/cm) used to accelerate the ions in the beam effectively quenches the metastables soon after they leave the ion source.

The only remaining excited He⁺ ions that reach the collision center must then be in high-lying Rydberg states. An analysis of the rate at which such states are produced under the conditions present in our rf ion source indicates that the fraction of the ions produced in the $9p$ state in the ion source is about 0.15%. Since transition rates into excited states decrease as n^{-3} , the initial population of higher- n states is very

small and field ionization in the accelerator further depletes these states. A worst-case calculation shows that the total fraction of ions with $n \geq 9$ reaching the collision center is smaller than 0.4%. Even though Rydberg-ion collisions have a greater probability of producing secondary electrons, we do not believe that the fraction of beam ions in such states is large enough to have an appreciable effect on the results.

III. RESULTS

Tables I–V list the DDCS's, the single-differential cross sections (SDCS's) integrated over either angle or energy, and the TICS's for the five incident energies measured. Examples of the 67- and 95-keV DDCS's are shown in Fig. 1 where they are compared with plane-wave Born approximation

TABLE II. Same as Table I for 48-keV He⁺+H₂.

| W (eV) | 15° | 30° | 50° | 70° | 90° | 110° | 130° | 160° | $\sigma(W)$ |
|------------------|----------|----------|----------|----------|----------|----------|----------|----------|-------------|
| 1.5 | 745 | 247 | 95.5 | 61.5 | 45.2 | 49.1 | 44.4 | 43.0 | 1230 |
| 2 | 643 | 190 | 81.8 | 52.8 | 39.1 | 46.4 | 43.0 | 40.2 | 1060 |
| 3 | 512 | 149 | 75.1 | 45.8 | 32.9 | 40.2 | 37.3 | 35.7 | 889 |
| 5 | 247 | 136 | 67.4 | 38.6 | 26.6 | 28.8 | 29.4 | 25.9 | 655 |
| 7.5 | 220 | 124 | 53.1 | 28.0 | 19.2 | 17.4 | 15.5 | 13.9 | 501 |
| 10 | 196 | 107 | 39.3 | 18.5 | 12.4 | 9.99 | 8.85 | 9.84 | 382 |
| 15 | 135 | 72.6 | 22.4 | 9.41 | 5.81 | 4.25 | 5.39 | 3.23 | 230 |
| 20 | 85.6 | 44.7 | 1.32 | 5.52 | 3.09 | 4.02 | 1.8 | 1.6 | 138 |
| 30 | 33.0 | 17.5 | 5.30 | 2.03 | 1.61 | 0.624 | 0.500 | 0.453 | 52.6 |
| 50 | 5.26 | 2.85 | 3.44 | 0.356 | 0.143 | 0.0771 | 0.0609 | 0.0422 | 12.8 |
| 75 | 1.83 | 0.396 | 0.117 | 0.0370 | 0.0146 | 9.34[-3] | 8.19[-3] | 7.86[-3] | 1.63 |
| 100 | 0.101 | 0.0592 | 0.0155 | 3.68[-3] | 2.36[-3] | 1.17[-3] | 1.11[-3] | 1.30[-3] | 0.152 |
| 130 | 0.0114 | 6.59[-3] | 2.14[-3] | 6.10[-4] | 3.37[-4] | 1.70[-4] | 1.53[-4] | 2.89[-4] | 0.0186 |
| 160 | 1.72[-3] | 1.03[-3] | 2.70[-4] | | | | | 2.17[-4] | 3.40[-3] |
| 200 | 1.49[-4] | 1.04[-4] | 4.27[-4] | | | | | 1.93[-4] | 1.49[-3] |
| $\sigma(\theta)$ | 6150 | 2800 | 1120 | 557 | 385 | 368 | 341 | 317 | 11 400 |

TABLE III. Same as Table I for 67-keV $\text{He}^+ + \text{H}_2$.

| W (eV) | 15° | 30° | 50° | 70° | 90° | 110° | 130° | 160° | $\sigma(W)$ |
|------------------|----------|----------|----------|----------|----------|----------|----------|----------|-------------|
| 1.5 | 803 | 324 | 104 | 60.0 | 40.4 | 41.6 | 34.4 | 46.3 | 1300 |
| 2 | 726 | 258 | 89.0 | 52.2 | 36.3 | 37.3 | 32.0 | 32.6 | 1120 |
| 3 | 660 | 210 | 79.1 | 45.1 | 29.1 | 31.6 | 27.5 | 25.6 | 967 |
| 5 | 502 | 174 | 73.0 | 38.5 | 25.3 | 22.6 | 21.0 | 19.0 | 785 |
| 7.5 | 346 | 171 | 67.8 | 32.8 | 20.4 | 16.0 | 14.1 | 15.4 | 642 |
| 10 | 333 | 164 | 55.9 | 24.4 | 15.1 | 10.1 | 10.5 | 8.91 | 553 |
| 15 | 283 | 133 | 35.6 | 12.4 | 7.37 | 7.33 | 3.98 | 3.34 | 395 |
| 20 | 210 | 96.9 | 22.6 | 7.94 | 4.42 | 3.39 | 2.14 | 2.02 | 274 |
| 30 | 98.3 | 44.7 | 9.25 | 3.09 | 2.50 | 0.973 | 0.733 | 0.772 | 123 |
| 50 | 16.5 | 6.79 | 3.23 | 0.616 | 0.255 | 0.143 | 0.115 | 0.114 | 22.7 |
| 75 | 8.21 | 2.64 | 0.248 | 0.0858 | 0.0366 | 0.0201 | 0.0164 | 0.0402 | 7.33 |
| 100 | 0.316 | 0.168 | 0.0486 | 0.0153 | 7.35[-3] | 3.75[-3] | 2.60[-3] | 4.64[-3] | 0.465 |
| 130 | 0.0427 | 0.0258 | 8.03[-3] | 2.42[-3] | 2.30[-4] | 7.23[-4] | 4.24[-4] | 9.27[-4] | 0.0682 |
| 160 | 7.57[-3] | 5.03[-3] | 1.72[-3] | 6.35[-4] | 8.46[-4] | 1.09[-4] | 1.66[-4] | 5.78[-4] | 0.0160 |
| 200 | 6.91[-4] | 8.89[-4] | 9.97[-4] | 5.92[-5] | 2.27[-4] | 3.07[-4] | 5.17[-5] | 1.96[-4] | 4.45[-3] |
| 250 | 3.62[-4] | 1.06[-4] | 2.77[-4] | | | | | 1.36[-4] | 9.38[-4] |
| 300 | 3.36[-5] | 1.77[-5] | 6.51[-5] | | | | | 9.13[-5] | 2.60[-4] |
| $\sigma(\theta)$ | 10 700 | 4600 | 1420 | 633 | 406 | 345 | 289 | 318 | 15 900 |

(PWBA) calculations [18] for protons of 17.5 keV (the same velocity as 70-keV He^+) incident on H_2 . Comparison is also made with experimental $\text{H}^+ + \text{H}_2$ data [13] at 20 keV.

Except for the 95-keV 130° spectrum from He^+ which differs because of Doppler-shifted autoionization peaks at energies below 10 eV, the equivelocity H^+ and He^+ cross sections agree fairly well at low energies. However, they differ by factors of 10 or more at higher energies. For the close collisions which produce fast electrons, the effective nuclear charge of the He^+ can be as large as 2 but even if the cross sections scaled as Z_{eff}^2 this would account for only a factor of 4. Electron loss from the projectile must account for the remaining discrepancy. In the following paper [14] cal-

culations for $\text{He}^+ + \text{H}$ are presented which show that electron loss dominates the energy spectrum at high energies; a situation which probably also holds for other targets. Except in the forward direction, the PWBA yields too large a cross section at low electron ejection energies and values which are too low at high energies. The failure of the PWBA is not surprising at these low incident ion velocities.

The peaks seen, e.g., at 75 eV in the 67-keV 15° data and at 20 eV in the 95-keV 90° curve are due to autoionization (AI) from doubly excited states of helium. The peaks, which come at about 35 eV in the reference frame of the emitter, are Doppler shifted [19] due to the motion of the projectiles. Figure 2 shows the AI peaks in more detail with the expected

TABLE IV. Same as Table I for 95-keV $\text{He}^+ + \text{H}_2$.

| W (eV) | 15° | 30° | 50° | 70° | 90° | 110° | 130° | 160° | $\sigma(W)$ |
|------------------|----------|----------|----------|----------|----------|----------|----------|----------|-------------|
| 1.5 | 1080 | 480 | 141 | 63.7 | 37.4 | 43.7 | 41.1 | 42.1 | 1300 |
| 2 | 984 | 394 | 117 | 54.5 | 31.6 | 39.0 | 35.0 | 34.6 | 1120 |
| 3 | 860 | 313 | 96.3 | 43.2 | 25.2 | 31.9 | 27.9 | 26.9 | 967 |
| 5 | 725 | 239 | 80.8 | 34.2 | 20.1 | 22.2 | 20.1 | 22.4 | 785 |
| 7.5 | 570 | 202 | 71.3 | 29.1 | 16.4 | 15.2 | 16.9 | 12.6 | 642 |
| 10 | 455 | 192 | 66.6 | 24.5 | 13.5 | 13.4 | 10.9 | 8.49 | 553 |
| 15 | 401 | 180 | 50.0 | 15.3 | 7.93 | 7.03 | 4.61 | 4.23 | 395 |
| 20 | 347 | 156 | 35.0 | 9.55 | 8.42 | 3.49 | 2.66 | 2.50 | 274 |
| 30 | 221 | 96.2 | 17.2 | 4.58 | 2.35 | 1.60 | 1.28 | 1.20 | 123 |
| 50 | 57 | 23.5 | 3.50 | 0.997 | 0.490 | 0.345 | 0.317 | 0.290 | 22.7 |
| 75 | 6.58 | 10.2 | 0.577 | 0.152 | 0.076 6 | 0.057 5 | 0.053 0 | 0.047 1 | 7.33 |
| 100 | 1.09 | 0.486 | 0.118 | 0.038 5 | 0.017 9 | 0.012 1 | 0.009 41 | 0.008 16 | 0.465 |
| 130 | 0.158 | 0.078 9 | 0.022 0 | 0.007 85 | 0.003 23 | 0.001 84 | 0.001 88 | 0.001 80 | 0.068 2 |
| 160 | 0.031 5 | 0.016 9 | 0.006 37 | 0.001 69 | 0.001 24 | 1.93[-4] | 9.06[-4] | 7.83[-4] | 0.016 0 |
| 200 | 0.005 16 | 0.003 25 | 8.89[-4] | 6.41[-4] | 3.88[-4] | 5.67[-5] | 4.11[-4] | 3.55[-4] | 0.004 45 |
| 250 | 6.31[-4] | 6.19[-4] | | | | | | 1.39[-4] | 9.38[4] |
| 300 | 1.45[-4] | 7.07[-5] | | | | | | | 2.60[-4] |
| $\sigma(\theta)$ | 17 200 | 7380 | 1890 | 682 | 392 | 379 | 333 | 322 | 15 900 |

TABLE V. Same as Table I for 114-keV $\text{He}^+ + \text{H}_2$.

| W (eV) | 15° | 30° | 50° | 70° | 90° | 110° | 130° | 160° | $\sigma(W)$ |
|------------------|----------|----------|----------|----------|----------|----------|----------|----------|-------------|
| 1.5 | 1400 | 620 | 197 | 89.2 | 51.5 | 39.7 | 35.9 | 33.3 | 2110 |
| 2 | 1280 | 520 | 174 | 79.1 | 43.1 | 35.6 | 31.2 | 30.7 | 1850 |
| 3 | 1030 | 392 | 131 | 62.7 | 34.3 | 28.3 | 24.5 | 26.0 | 1450 |
| 5 | 773 | 266 | 90.0 | 38.3 | 21.6 | 18.0 | 19.1 | 16.6 | 1010 |
| 7.5 | 640 | 211 | 75.8 | 29.3 | 15.5 | 13.8 | 11.8 | 9.91 | 805 |
| 10 | 513 | 190 | 65.7 | 23.5 | 12.3 | 10.7 | 7.37 | 6.93 | 666 |
| 15 | 418 | 180 | 55.5 | 17.5 | 9.20 | 5.71 | 4.53 | 4.16 | 555 |
| 20 | 383 | 153 | 38.2 | 9.98 | 6.93 | 3.19 | 2.32 | 2.20 | 449 |
| 30 | 268 | 108 | 20.5 | 7.59 | 2.53 | 1.49 | 1.15 | 1.08 | 297 |
| 50 | 91.9 | 32.4 | 5.38 | 1.29 | 0.655 | 0.423 | 0.342 | 0.301 | 91.1 |
| 75 | 15.0 | 9.08 | 0.824 | 0.240 | 0.127 | 0.083 9 | 0.072 8 | 0.064 5 | 18.5 |
| 100 | 5.08 | 0.849 | 0.164 | 0.047 5 | 0.027 7 | 0.019 4 | 0.014 2 | 0.011 6 | 3.83 |
| 130 | 0.333 | 0.130 | 0.031 5 | 0.010 9 | 0.005 15 | 0.003 47 | 0.002 92 | 0.002 10 | 0.391 |
| 160 | 0.063 8 | 0.027 7 | 0.008 51 | 0.002 94 | 0.001 28 | 5.86[-4] | 7.37[-4] | 4.69[-4] | 0.084 7 |
| 200 | 0.010 1 | 0.005 31 | 0.001 69 | 6.34[-4] | 3.56[-4] | 4.33[-5] | 1.07[-4] | 2.06[-4] | 0.015 6 |
| 250 | 0.001 50 | 9.25[-4] | 3.55[-4] | 1.81[-4] | | | | 6.21[-5] | 0.002 68 |
| 300 | 3.20[-4] | 1.89[-4] | 4.72[-5] | | | | | | 4.19[-4] |
| $\sigma(\theta)$ | 20 800 | 8290 | 2230 | 848 | 449 | 331 | 286 | 263 | 26 300 |

positions of the transitions from the four most prominent states $2s^2\ ^1S$, $2s2p\ ^3P$, $2s2p\ ^1P$, and $2p^2\ ^1S$ [20] marked with vertical lines. The Doppler-shifted AI peaks also appear in the angular distributions of the DDCS's as seen in Fig. 3 where three examples are marked with lines representing the approximate expected positions. To make a closer examination of the spectrum of the AI electrons would require finer angular steps and better angular and energy resolution.

The sizes of the AI peaks seemed unexpectedly large since they must be due to collisions in which the He^+ ion either captures one electron into an excited state with a simultaneous excitation of the other or else captures an electron in one collision and then has a second collision in which two electrons are simultaneously excited. Since the fraction of beam particles already neutralized before reaching the collision center is estimated to be less than 5%, the contribution due to the second mechanism should be small. To quantify

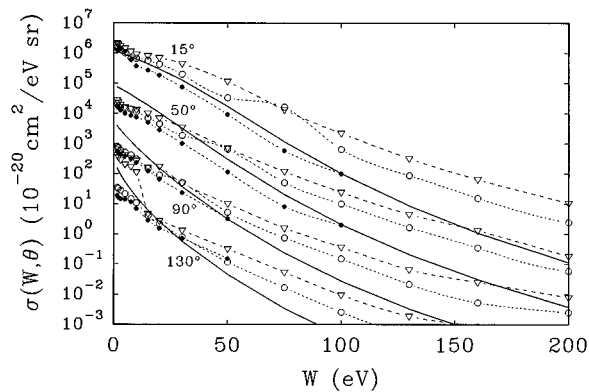


FIG. 1. DDCS's at four angles. \circ , present data for 67-keV $\text{He}^+ + \text{H}_2$; ∇ , present data for 95-keV $\text{He}^+ + \text{H}_2$; \bullet , data of Gealy *et al.* [13] for $\text{H}^+ + \text{H}_2$ at 20 keV; solid line, PWBA calculations for $\text{H}^+ + \text{H}_2$ at 17.5 keV. Plots at 15°, 50°, and 90° have been multiplied by 2000, 200, and 20, respectively, to reduce overlap.

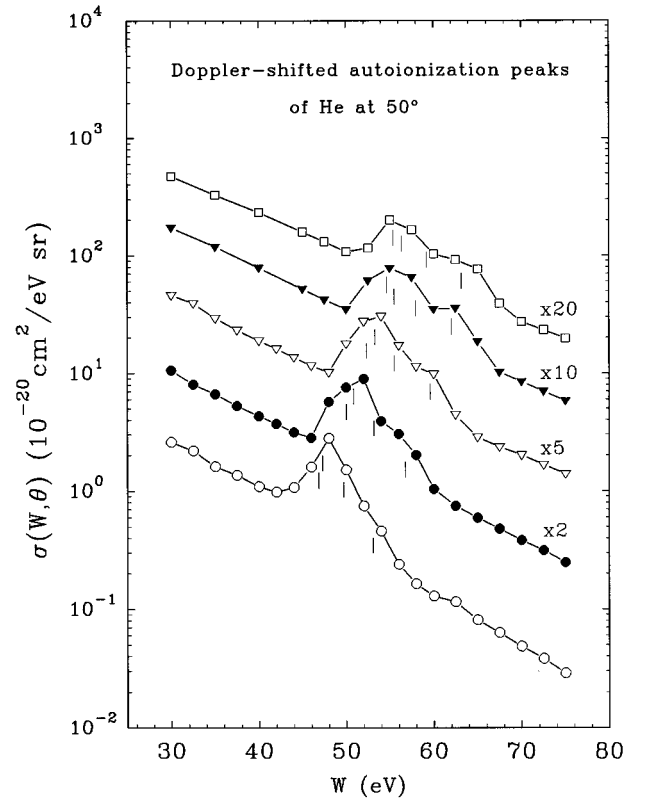


FIG. 2. Spectra of electrons ejected at 50° from $\text{He}^+ + \text{H}_2$ collisions showing Doppler-shifted autoionization peaks. The incident ion energies were, from top to bottom, 114, 95, 67, 48, and 28 keV and the data were multiplied by the stated factors to avoid overlap. The expected positions of the AI transitions from the $2s^2\ ^1S$, $2s2p\ ^3P$, $2s2p\ ^1P$, and $2p^2\ ^1S$ states are shown by the vertical lines.

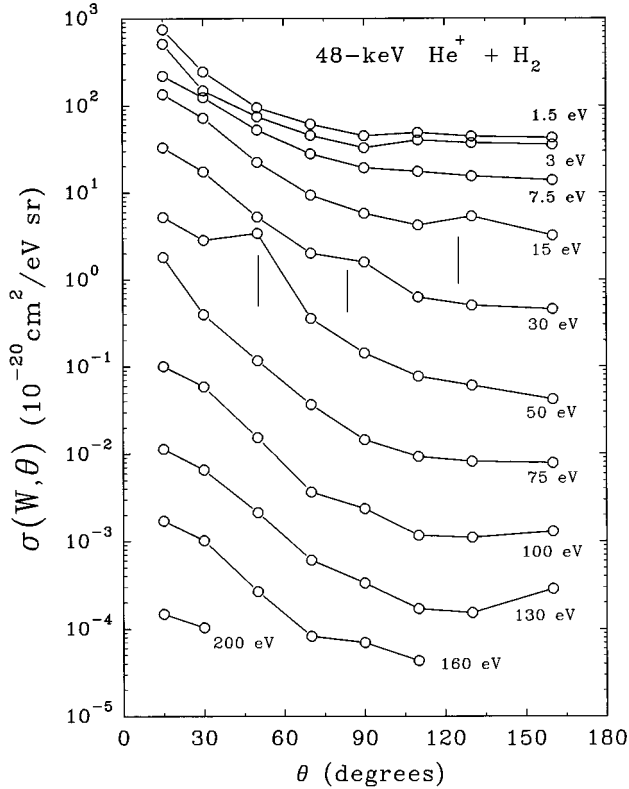


FIG. 3. Angular distributions of electrons of various energies from 48-keV $\text{He}^+ + \text{H}_2$ collisions. Expected positions of the Doppler-shifted helium autoionization peaks are indicated by vertical lines.

the contribution of AI, the cross section for 114-keV impact energy and 50° ejection angle was determined for the sum of the four AI transitions by integrating the part of the curve in that region in excess of a smooth curve representing the continuum. The resulting cross section was $7.3 \times 10^{-19} \text{ cm}^2/\text{sr}$ with an uncertainty of about 15%. From the work of Schowengerdt, Smart, and Rudd [21] we can estimate the cross section for the sum of the same four AI peaks for 60-keV $\text{H}_2^+ + \text{He}$. This corresponds approximately to the same impact velocity and is the same collision pair except for the interchange of charge states. The result for $\text{H}_2^+ + \text{He}$ is $5.8 \times 10^{-20} \text{ cm}^2/\text{sr}$, which is smaller by a factor of 12 or 13 than the $\text{He}^+ + \text{H}_2$ AI cross section from the present measurement. While this comparison was done only at 50° , the results would not be much different at any other angle. This is a strong indication that for this collision pair simultaneous capture and double excitation is a much more likely process than an ordinary double excitation.

Integration of the DDCS's over all directions yields the SDCS's which describe the overall energy spectrum of electrons. These results are shown in Fig. 4 where they are plotted as ratios of the measured SDCS's to the Rutherford cross sections calculated from Eq. (4) in paper I [13]. This is a common way of displaying such cross sections to reduce the large spread of values. Since no equivelocity proton impact data are available, comparison is made with a semiempirical model for proton impact [22,23] which has been found to represent the data reasonably well. Calculations on this model using the parameters given by Rudd *et al.* [23] for

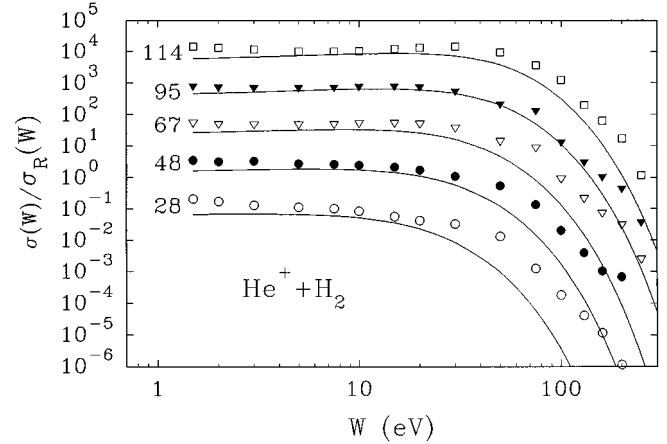


FIG. 4. Energy distributions of electrons from $\text{He}^+ + \text{H}_2$ collisions at various impact energies presented as SDCS's divided by the Rutherford cross section. Data points, present data; solid line, model calculations [22,23] for equivelocity H^+ impacts. Plots at 48, 67, 95, and 114 keV incident energies were multiplied by successive powers of 10 to reduce overlap.

$\text{H}^+ + \text{H}_2$ are shown as the lines. While the agreement is fair at intermediate ejected electron energies, it is seen that, as noted above for the DDCS's, the He^+ data are consistently higher than the H^+ cross sections at the higher ejected electron energies, particularly at the lower incident ion energies.

Comparison of the present TICS data with the results of more direct measurements by other methods provides a test of the overall accuracy of our measurements. In Fig. 5 our data are seen to be in excellent agreement with those of Solov'ev *et al.* [6] and with the recommended values given by McDaniel *et al.* [17].

IV. CONCLUSIONS

We have measured the angular and energy distribution of electrons from $\text{He}^+ + \text{H}_2$ collisions. The cross sections for He^+ collisions are larger than those for $\text{H}^+ + \text{H}_2$ collisions at the same projectile velocity, especially at the higher ejected

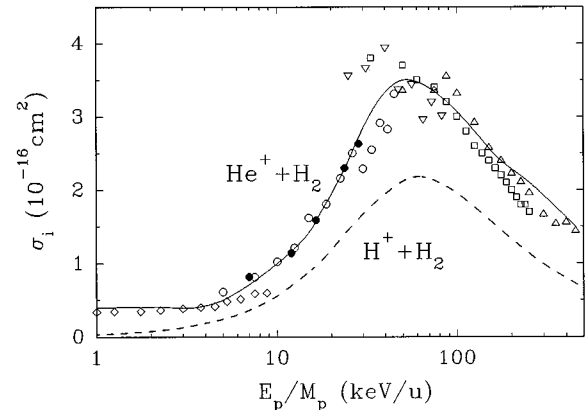


FIG. 5. TICS's for $\text{He}^+ + \text{H}_2$ collisions. \bullet , present data; \circ , data of Solov'ev *et al.* [6]; \diamond , data of Keene [7]; \triangle , data of Pivovar, Levchenko, and Grigor'ev [8]; \square , data of Langley *et al.* [9]; ∇ , data of Gilbody *et al.* [10]; solid line, recommended values [17]. The dashed line indicates $\text{H}^+ + \text{H}_2$ cross sections for comparison.

electron energies. While most of the difference can be attributed to electron emission from the projectile, some difference would be expected from the larger effective nuclear charge of the helium ion for the close collisions producing high-energy electrons. Born approximation calculations generally yield cross sections that are too large at low ejected electron energies and too small at high energies. The prominence of Doppler-shifted autoionization peaks from the he-

lium projectiles indicates a substantial probability for simultaneous excitation and capture to excited states.

ACKNOWLEDGMENT

This work was supported by National Science Foundation Grant Nos. PHY9020529 and PHY9119818.

-
- [1] W. E. Wilson and L. H. Toburen, *Phys. Rev. A* **7**, 1535 (1973).
- [2] D. Burch, H. Wieman, and W. B. Ingalls, *Phys. Rev. Lett.* **30**, 823 (1973).
- [3] F. Drepper and J. S. Briggs, *J. Phys. B* **9**, 2063 (1976).
- [4] M. E. Rudd, J. S. Risley, J. Fryar, and R. G. Rolles, *Phys. Rev. A* **21**, 506 (1980).
- [5] R. E. Olson, J. Ullrich, and H. Schmidt-Böcking, *J. Phys. B* **20**, L809 (1987).
- [6] S. Solov'ev, R. N. Il'in, V. A. Oparin, and N. V. Fedorenko, in *Atomic Collision Processes*, edited by M. R. C. McDowell (North-Holland, Amsterdam, 1964).
- [7] B. Keene, *Philos. Mag.* **40**, 369 (1949).
- [8] L. I. Pivovarov, Yu. Z. Levchenko, and A. N. Grigor'ev, *Zh. Eksp. Teor. Fiz.* **54**, 1310 (1968) [*Sov. Phys. JETP* **27**, 699 (1968)].
- [9] R. A. Langley, Ph.D. thesis, Georgia Institute of Technology, 1964 (unpublished). See also R. A. Langley, D. W. Martin, D. S. Harmer, J. W. Hooper, and E. W. McDaniel, *Phys. Rev.* **136**, A379 (1964).
- [10] H. B. Gilbody, J. B. Hasted, J. V. Ireland, A. R. Lee, E. W. Thomas, and A. S. Whiteman, *Proc. R. Soc. London Ser. A* **274**, 40 (1963).
- [11] N. Oda and F. Nishimura, in *Abstracts of the XIth International Conference on the Physics of Electronic and Atomic Collisions, Kyoto, 1979*, edited by K. Takayanagi and N. Oda (The Society for Atomic Collisions Research, Kyoto, 1979), p. 622.
- [12] A. Kövér, A. Ricz, Gy. Szabó, D. Berényi, E. Koltay, and J. Végh, *Phys. Lett.* **79A**, 305 (1980).
- [13] M. W. Gealy, G. W. Kerby III, Ying-Yuan Hsu, and M. E. Rudd, *Phys. Rev. A* **51**, 2247 (1995) (paper I).
- [14] Ying-Yuan Hsu, M. W. Gealy, G. W. Kerby III, and M. E. Rudd, following paper, *Phys. Rev. A* **53**, 303 (1996).
- [15] N. Stolterfoht, D. Schneider, D. Burch, H. Wieman, and J. S. Risley, *Phys. Rev. Lett.* **33**, 59 (1974).
- [16] S. T. Manson and L. H. Toburen, *Phys. Rev. Lett.* **46**, 529 (1981).
- [17] E. W. McDaniel, M. R. Flannery, H. W. Ellis, F. L. Eisele, and W. Pope, High Energy Laser Laboratory, U.S. Army Missile Research and Development Command, Technical Report No. H-78-1, Vol. I, 1977 (unpublished).
- [18] C. E. Kuyatt and T. Jorgensen, Jr., *Phys. Rev. A* **130**, 1444 (1963).
- [19] M. E. Rudd, T. Jorgensen, Jr., and D. J. Volz, *Phys. Rev. Lett.* **16**, 929 (1966).
- [20] M. E. Rudd, *Phys. Rev. Lett.* **13**, 503 (1964).
- [21] F. D. Schowengerdt, S. R. Smart, and M. E. Rudd, *Phys. Rev. A* **7**, 560 (1973).
- [22] M. E. Rudd, *Phys. Rev. A* **38**, 6129 (1988).
- [23] M. E. Rudd, Y.-K. Kim, D. H. Madison, and T. J. Gay, *Rev. Mod. Phys.* **64**, 441 (1992).